THE INTERNATIONAL JOURNAL OF MEDICAL ROBOTICS AND COMPUTER ASSISTED SURGERY
Int J Med Robotics Comput Assist Surg 2011; **7**: 304–317.
Published online 11 May 2011 in Wiley Online Library (wileyonlinelibrary.com) **DOI:** 10.1002/rcs.399

ORIGINAL ARTICLE

Graphic and haptic simulation system for virtual laparoscopic rectum surgery

Jun J. Pan[1]*
Jian Chang[1]
Xiaosong Yang[1]
Jian J. Zhang[1]
Tahseen Qureshi[2]
Robert Howell[3]
Tamas Hickish[3]

[1]*National Centre for Computer Animation, Media School, Bournemouth University, UK*

[2]*Poole Hospital, Poole, UK*

[3]*Royal Bournemouth and Christchurch Hospitals, Bournemouth, UK*

*Correspondence to: Jun J. Pan, National Centre for Computer Animation, Media School, Bournemouth University, UK.
E-mail: pjunjun@bournemouth.ac.uk

Accepted: 1 April 2011

Abstract

Background Medical simulators with vision and haptic feedback techniques offer a cost-effective and efficient alternative to the traditional medical trainings. They have been used to train doctors in many specialties of medicine, allowing tasks to be practised in a safe and repetitive manner. This paper describes a virtual-reality (VR) system which will help to influence surgeons' learning curves in the technically challenging field of laparoscopic surgery of the rectum.

Methods Data from MRI of the rectum and real operation videos are used to construct the virtual models. A haptic force filter based on radial basis functions is designed to offer realistic and smooth force feedback. To handle collision detection efficiently, a hybrid model is presented to compute the deformation of intestines. Finally, a real-time cutting technique based on mesh is employed to represent the incision operation.

Results Despite numerous research efforts, fast and realistic solutions of soft tissues with large deformation, such as intestines, prove extremely challenging. This paper introduces our latest contribution to this endeavour. With this system, the user can haptically operate with the virtual rectum and simultaneously watch the soft tissue deformation.

Conclusions Our system has been tested by colorectal surgeons who believe that the simulated tactile and visual feedbacks are realistic. It could replace the traditional training process and effectively transfer surgical skills to novices.

Keywords cutting algorithm; haptic force filter; laparoscopic rectum surgery; virtual reality

Introduction

In recent times, minimally invasive techniques have revolutionized many surgical procedures. Compared with traditional open surgery, minimally invasive surgery (MIS) is associated with a reduction in surgical trauma, less postoperative pain with fewer complications and a shorter convalescence for patients. In the last decade, laparoscopic colorectal surgery in particular has witnessed a shift from open surgery to the laparoscopic approach for colorectal surgery, supported by clinical trial evidence.

Colorectal cancer is the third commonest cancer in the UK, with approximately 40,000 new cases diagnosed every year. Surgery remains the mainstay of treatment and is the primary intervention in 80% of cases. Although it

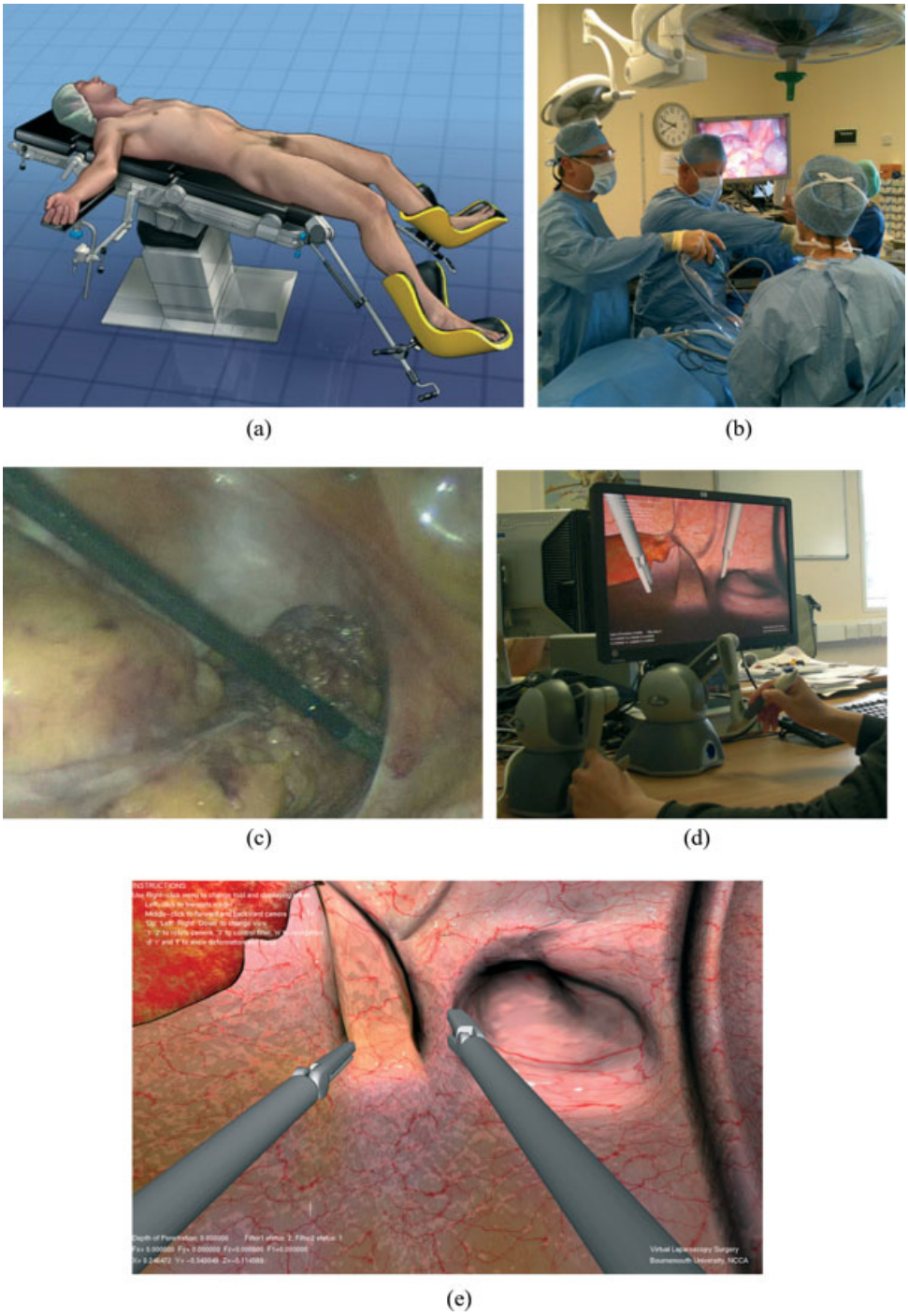

Figure 1. Comparison of real laparoscopic rectum surgery with our VR-based simulation system: (a) modified Lloyd-Davies position; (b) real operation environment for laparoscopic rectum surgery; (c) screen shot from real surgery video; (d) virtual haptic device and PC; (e) snapshot of our VR-based simulator

is estimated that 90% of cases are suitable for a laparoscopic approach, at present there is a relative lack of surgeons trained to perform such demanding surgery. This is particularly true for rectal cancer surgery, which is the most complex and technically challenging for the laparoscopic colorectal surgeon.

The preoperative diagnosis and preparation is the same as for open surgery (1). An endoscopy enables histological confirmation of cancer as well as information on its position within the rectum. A CT scan will provide evidence of spread to distant organs, such as the liver and lungs. In addition, recommendations are that patients with rectal cancer have an MRI scan, providing particular information on the local extent of the cancer. This helps with the formulation of a plan of treatment, particularly whether surgery should be proceeded by chemoradiotherapy. During the operation, patients are placed in a modified Lloyd–Davis position (Figure 1a). The number of operating ports inserted varies between surgeons, but typically four ports are used. The operating

DOI: 10.1002/rcs

assistant is required to control the camera and help with the retraction of tissues during the procedure. The surgeon relies on a variety instruments, including energy sources, clips and stapling devices to help dissect, seal and divide tissues. The greatest challenge and eventual goal of surgery is to separate the rectum, complete with its envelope of fat (mesorectum), from the surrounding pelvic structures. The specimen can then be delivered from the patient through an extraction site either in the left iliac fossa or via a Pfannensteil incision. The incision is shielded with a wound protector to help prevent implantation of tumour cells. Figure 1b shows the theatre set up for a laparoscopic resection; Figure 1c gives a typical view the surgeon will have during laparoscopic rectal cancer surgery.

At present, trainee laparoscopic surgeons will try to influence their learning curves by the use of training boxes. These can contain inanimate objects, which offer only mundane tasks and lack the feel of handling real tissue. Animal tissue may be used but differs in anatomy to humans. Cadaveric courses are available but are expensive and, by their nature, do not allow repetitive tasks to be performed. In reality, therefore, trainees in many countries, including the UK, develop their laparoscopic skills by operating directly on patients under the tutelage of senior surgeons. Virtual reality simulators would have the potential to shorten the surgeons' learning curves, allowing a procedure to be performed in a repetitive manner, at the same time familiarizing the trainee with the anatomy for that particular procedure. We feel that VR simulators have become a viable alternative in recent years, allowing the trainee surgeon to hone his or her skills by operating on a virtual patient. Compared with traditional surgical training on patients, VR-based methods provide the following:

1. *Repetitive tasks*: a VR-based system can be reused many times without risk to patients.
2. *Variable complexity*: different scenarios can be simulated, including extreme situations, allowing the response to be rehearsed.
3. *Surgeon responses can be recorded*: skills and training progress can be objectively recorded, measured and evaluated.

At present, there are a number of VR-based laparoscopic surgery simulators available. including some commercial products, such as CAE (2) and Xitact (3). However, these simulators primarily focus on operations where there are only small deformations and movements of soft tissues, such as gall bladder removal (cholecystectomy), resection of ectopic pregnancy and knee surgery. Colorectal cancer surgery, however, is very different because of the substantial soft tissue movement and deformation. It therefore presents a much greater challenge for the computation of realistic deformations and haptic response. Moreover, as the bowel and other soft tissues at the proximity frequently self-collide and collide with the abdominal cavity during operation, an efficient collision detection algorithm is also essential to robustly detect collisions in real time.

A great deal of research effort has been made in VR-based medical simulation in the recent years. Heng *et al*. (4) presented a virtual reality training system for knee arthroscopic surgery. They added some DC servo-motors to the haptic device with increased degrees of freedom (DOFs). The virtual models were developed based on the Visible Human Project dataset. The deformation and the real-time cutting of soft tissues were simulated using finite element analysis (FEA). As only small soft tissue movement was involved in this simulator, deformation was not the main concern. Choi *et al*. (5) developed a VR-based simulator for laparoscopic oesophagus surgery. In their system, the cutting of soft tissue in the oesophagus is implemented with geometric organ models segmented from the Visible Human Dataset. The boundary element method (BEM) was used to compute the deformation with linear response assumptions. The mechanical parameters (elastic modulus and Poisson's coefficient) were obtained from animal experiments and integrated with graphic and haptic devices. Although the computation speed of this simulator can be ensured with linear response assumptions, it can not cope with large deformations, since the model behaviour may diverge. Several research groups, such as INRIA have recently attempted to model intestine deformation (7–9). One idea is to represent the global deformation of the intestine by its medial axis (centre line) to simplify the shape change of the cross-section. Li *et al*. (6) used Laplacian coordinates to drive the mesh deformation consistently with the centre line. However, the surface deformation of this method cannot be made in real time. France *et al*. (7) represented the medial axis of the intestine with a physical spline constructed by Lagrangian dynamics. Because it is efficient to use a 1D curve to capture the deformation, smoothing skinning (8,9) was used to generate deformations of a 3D mesh for an intestine, following the shape of its centre line. However, the smooth skinning method suffers from some important drawbacks, such as 'collapsing joints' and 'candy-wrapper artefacts' (10). Haptic rendering (11–13) is another important research topic in VR-based medical simulation. Basdogan *et al*. (14) gave a framework to survey all the important aspects of haptic device in minimally invasive surgical simulation and training, including haptic recording, interface and rendering. Wu *et al*. (15) presented a method to generate smooth feedback force in haptic interaction with coarse polygonal meshes. It calculates the interaction force based on the Gregory patches, which are locally constructed from n-sided polygons and preserve the continuity across patch boundaries. During real-time haptic interaction, as the contact point is continuously tracked on the locally constructed Gregory patches, the renewed haptic forces are smooth. Maciel *et al*. (16) presented a dynamic point algorithm for line-based collision detection in haptics. In many cases, the surgical instruments are long slender objects. Here authors treated the surgical instruments as a line with its end points; a dynamic point is located

DOI: 10.1002/rcs

between the end points and the dynamic point is the closest point on the line to collide with model potentially. To deal with multiple contacts and non-convexities, the line is decomposed into segments and a dynamic point is applied for each segment. With a near-constant complexity, it can efficiently compute the interaction between a line-shaped haptic cursor and model surface.

This paper describes a VR-based simulation system for laparoscopic rectum surgery. We selected surface mesh rather than tetrahedra to represent the intestine model in the system, for two reasons. First, considering the unique deformation characteristics of colorectal cancer surgery as discussed above, it is difficult to perform good haptic rendering with volume data model at a 1 kHz rate using the current computing hardware; a surface model requires less computation. Second, in rectal surgery the manipulations mostly involve cutting the membrane and fat tissues connected surrounding the intestine. These membranes are very thin structures and shrink after an incision. In this sense, a surface model is more suitable to represent the physical behaviour of membranes than a volumetric model. In our simulator, the surface mesh model of an intestine was constructed with reference to the MRI data and real surgery videos. Basically, the force from the haptic device (Phantom Omni) applies to one point at an instant during manipulation; it can lead to deformation and shape distortion of the soft tissue. To offer realistic and smooth force feedback and deformation, we have designed a haptic force filter based on the radial basis functions. It is able to adjust the force adaptively according to the mesh density of the contact surface. To meet the requirement of real-time graphic performance and high deformation accuracy, a Cosserat rod model has been introduced to cope with collision detection and physical deformation. It parameterizes the centre line of the intestine with material coordinates, which are moving along with the deforming structure. Rigid spheres are attached to the Cosserat rod, approximating the three-dimensional (3D) shape as bounding volumes of the intestine model for collision detection and deformation. This approach compares favourably with others with respect to computational efficiency and enables surface-based real-time cutting. Without major modification of the original mesh, new sub-triangles are created by a hierarchical method.

Materials and Methods

Interface and system architecture

Figure 1e is a snapshot of the interface of our VR-based simulation system. The interface shows a section of the rectum model and other soft tissue connected with the rectum. The hardware of our system is composed of a computer, a display screen and two haptic devices (Figure 1d). Usually, one haptic device functions as a grasping tool and the other is the harmonic scalpel. The haptic device (Phantom Omni) provides three-DOF

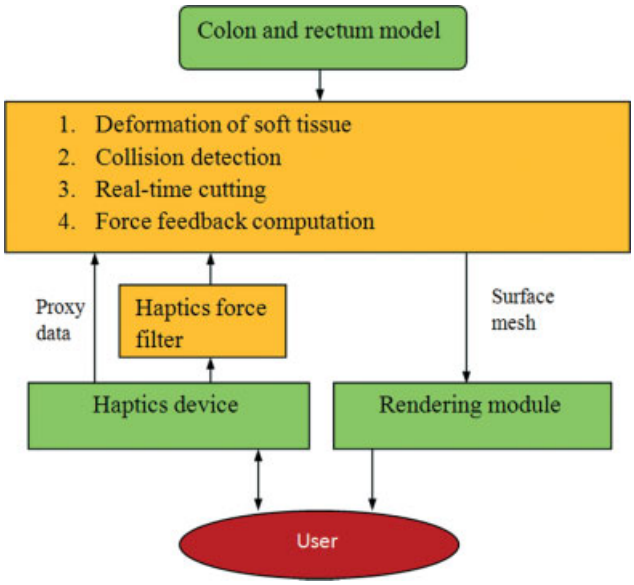

Figure 2. The system architecture of the VR-based laparoscopic rectum surgery simulator

navigating parameters (pitch, yaw and insertion) and force feedback when there is a collision detected. The user interface also permits use of the haptic device as a navigation camera.

The software was developed with OpenGL and C++. The overall system flow consists of two stages, preprocessing and a run-time operation. In the preprocessing stage, the 3D surface model of the colon and rectum are constructed using MRI data and real surgery videos. Using the MRI data supplied by the surgeons, we use the medical software package (3D Med 2.2) (17) to segment the image sequence and reconstruct a rough 3D colon and rectum model. By referencing the real surgery videos, a specific section of the bowel is selected and the connected membrane tissues are created manually. We use the triangle mesh model for the intestine, since it is simple and efficient in deformation computation. Run-time operations include soft tissue deformation, collision detection, cutting, rendering and communication with the haptic devices. According to the soft tissue deformation results, the interface procedure of the haptic device tracks the position and orientation of the proxy (haptic handle) and drives the haptic device to feed back force. The software architecture of our system is illustrated in Figure 2.

From the clinical aspect, the most important contribution we make is that it provides a comprehensive framework for virtual rectum surgery training, from system design to implementation. Compared with the other VR-based simulation systems (4,5), there are also three technical contributions:

1. A radial basis function-based haptic force filter offers realistic and smooth deformation in virtual operation.
2. A hybrid mechanical model of the intestine handles the soft tissue deformation and collision detection, which is both simple and efficient in computation.

DOI: 10.1002/rcs

3. A straightforward real-time cutting technique is developed, based on surface mesh. Without much modification of the original mesh, new sub-triangles are created and recorded in a hierarchical database to represent the cutting operation.

Haptic force filter

Theoretically, the force from the haptic device (Phantom Omni) applies to only one contact point during manipulation. In practice, however, the contact is an area, i.e. a contact surface between the intestine and surgical instruments, which can not be simplified as a single point, especially as the contact surface area changes from time to time. For example, for prodding and grasping, the contact surface is a face. If the contact surface is treated as a point, it can cause shape distortion and unsmoothness of the soft tissues, especially when the mesh is dense. To get around this problem, we present a simple but effective method called a 'radial basis function-based haptic force filter'. This filter can disperse the haptic force from one vertex to its neighborhood area with the function of force smoothing, making the graphic performance more realistic during manipulation.

Here, we use the Gaussian distribution function as our radial basis function, which can be described as follows:

$$F_i = AF_0 e^{-r^2/(2\sigma^2)} \tag{1}$$

where F_0 is the original force feedback applied on the contact vertex, r is the Euclidean distance in 3D space between the contact vertex and its neighbour vertex, i, and F_i is the filtered force which is dispersed from the contact vertex to its neighbour vertex i. The direction of F_i is the same as the direction of F_0. σ determines the range of the force filter. The bigger the value of σ is, the larger the affected range will be. A is the normalization coefficient, which makes the sum of the filtered force for all the vertices equal to F_0. Therefore A can be computed by the following formula:

$$A = \frac{F_0}{\sum F_0 e^{-r^2/(2\sigma^2)}} \tag{2}$$

In our simulator, we provide three grades for the haptic force filter for the user: 0, 1 and 2. For grade 0, the haptic force applies only on the contact vertex, which is the nearest vertex to the contact proxy. In this case, the filter has no effect. For grade 1, the haptic force is dispersed to the first circle of the neighbour vertices (Figure 3b). For grade 2, the haptic force is dispersed to the first and second circles of the neighbour vertices, which gives the largest filter range. Figure 3 gives an illustration of the ranges the filter covers.

In Figure 3, we use a needle to probe the surface of the intestine model. The left column shows the triangle mesh and all the vertices effect by the haptic forces. The pink point indicates the contact vertex. The yellow points indicate the first circle of neighbour vertices around the contact vertex. The blue points indicate the second circle of neighbour vertices. The values of the haptic forces of these vertices can be computed by (1), which is illustrated in the right column.

In a virtual operation, the system adaptively determines the filter grade by computing the area of contact surface between the surgery instrument and the intestine model. If the contact surface is smaller than the local average triangle area, the filter grade will be assigned as 0. If the contact surface is bigger than the local average triangle area and smaller than four times the local average triangle area, the filter grade will be assigned as 1. Then the contact vertex and its first circle of the neighbour vertices will be applied by the force. If the contact surface is bigger than four times the local average triangle area, the filter grade will be assigned as 2. Then the contact vertex and both the first and second circles of the neighbour vertices will be applied by the force. The criterion is summarized below:

$$\text{filter grade} = \begin{cases} 0, & \text{if} \quad S_{contact-surface} < S_{local-average-triangle} \\ 1, & \text{if} \quad S_{local-average-triangle} \le S_{contact-surface} \le 4S_{local-average-triangle} \\ 2, & \text{if} \quad S_{contact-surface} > 4S_{local-average-triangle} \end{cases} \tag{3}$$

Here, $S_{local-average-triangle}$ is the average area of all the neighbour triangles surrounding the contact vertex; $S_{contact-surface}$ is the area of contact surface. Here, we adopt the method mentioned in (16) to detect the collision between the surgery instrument and the intestine surface. When collision is detected, a simple but straightforward method is used to calculate the area of contact surface. We treat the tip of the surgery instrument as a cuboid (Figure 4). The areas of the three different rectangle surfaces of this cuboid are S_1, S_2 and S_3, respectively, and their normal vectors are n_1, n_2 and n_3. Suppose the normal vector of the contact triangle in the model mesh is n_0, then $S_{contact-surface}$ can be computed by:

$$S_{contact-surface} = w_1 S_1 |n_1 \cdot n_0| + w_2 S_2 |n_2 \cdot n_0| + w_3 S_3 |n_3 \cdot n_0| \tag{4}$$

where w_1, w_2 and w_3 are the weights. Our experience suggests that the following figures produce satisfactory results: $w_1 = 0.5$, $w_2 = 0.25$ and $w_3 = 0.25$. This process is illustrated in Figure 4.

Figure 5 illustrates the effect of the haptic force filter with different filter grades in a VR operation. We use a pair of forceps to grip the same area of an intestine tissue and pull it up with the same force. The deformed region enlarges as the filter grade increases. As the triangle mesh of this deformed intestine area is small compared with the contact surface of the surgery instrument, the result (see the tip of the clips) at Figure 5c looks more realistic than those at Figure 5a, b.

DOI: 10.1002/rcs

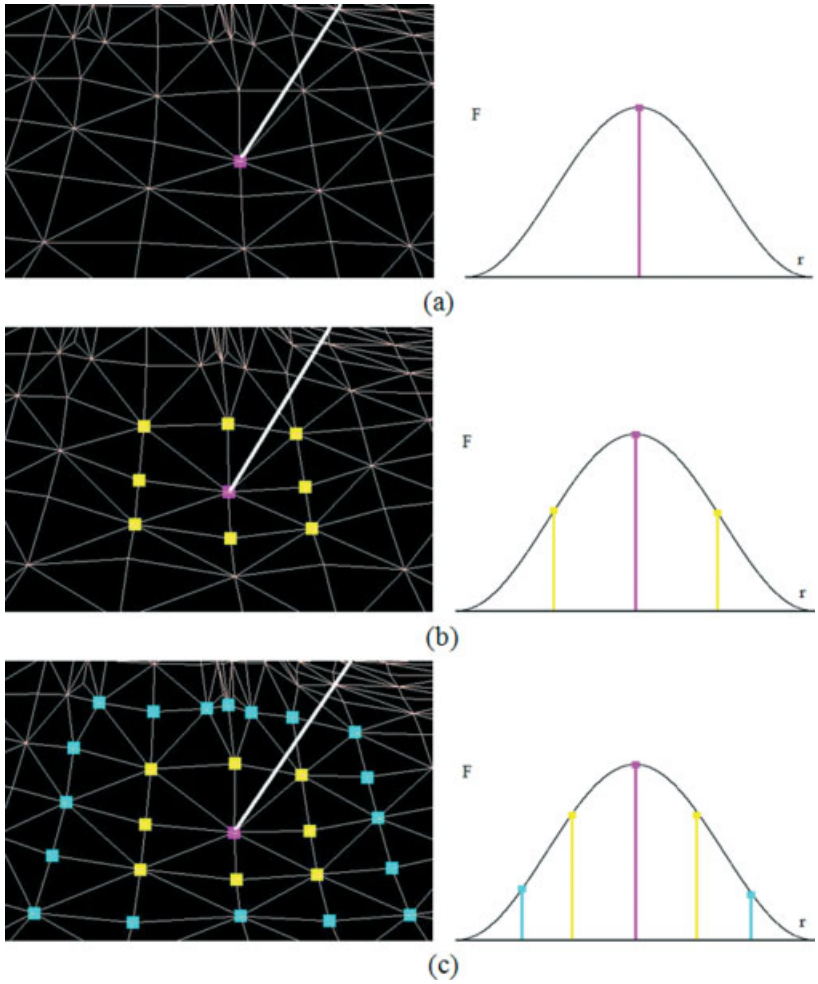

Figure 3. Force filter from grade 0 to 2: (a) grade 0; (b) grade 1; (c) grade 2

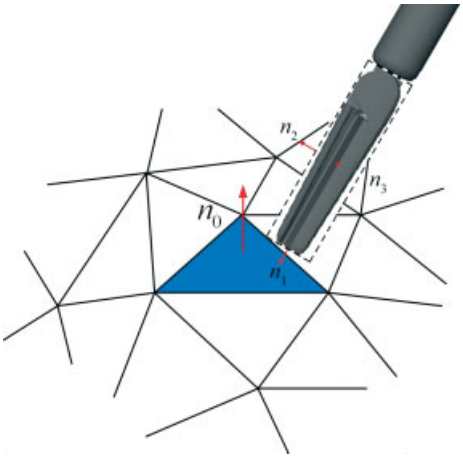

Figure 4. Computation of $S_{contact-surface}$ between the intestine model and a surgical instrument

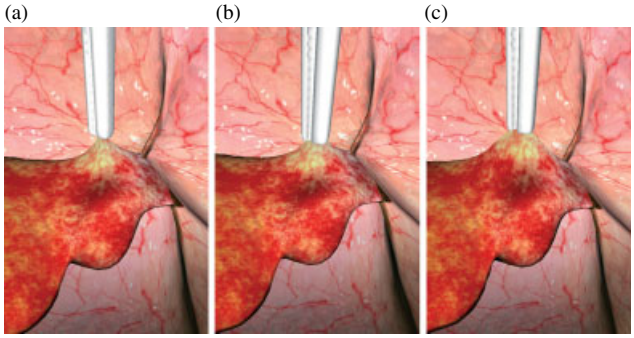

Figure 5. Pulling the same area of intestine tissue with different filter grades: (a) grade 0; (b) grade 1; (c) grade 2

Deformation and collision detection

For intestine surgery, as large movements and deformations of soft tissues take place during an operation, it is very challenging to compute realistic and real-time deformation. For soft tissue simulation, most current methods are based on the mass spring system (18,19) or the finite element method (20,21). The finite element method discretizes an object into many small elements and the solution is obtained by solving the governing partial differential equations. The finite element method can provide accurate results, especially when a large number of small elements are involved, but its computation complexity is usually high.

In our simulation system, we classify the deformation of different tissues into two types. For the membranes and fat tissues connected with the bowels, we use the

DOI: 10.1002/rcs

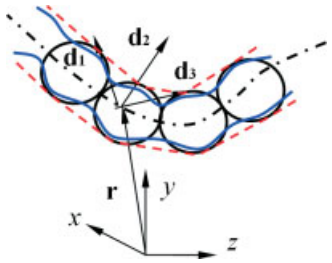

Figure 6. Illustration of hybrid deformation model

mass-spring model to simulate its behaviour. The mass spring system uses mass points to represent the volume or surface. The mass points are connected by springs to capture the dynamics. The advantage of a mass spring model is its computation efficiency. The implementation of mass spring system is straightforward and details can be found in related references (18). For the bowels, since they are long, thin, flexible objects, we take the advantage of modelling them as one-dimensional (1D) geometrical entities to efficiently extract their behaviours, including deformation computation and collision detection. We developed a hybrid mechanical model to describe the behaviour of intestines (rectums) in order to achieve fast simulation.

Hybrid deformation model

The hybrid model of rectum is illustrated in Figure 6. The deformation of the centre line is controlled by the mechanical model of the Cosserat rod (22). A string of spheres (black circles in Figure 6), which represent the approximated shape of the rectum, are rigidly attached to the centre line. The Cosserat rod represents a rod as a space curve with a local coordinate attached to each point of the curve. It can be bent and twisted. A cage (the red dashed line) is created to wrap the spheres. Since the spheres move and rotate with the centre line, the shape of the cage changes accordingly. The change of the cage is then mapped to the surface of the intestine model mesh (the blue solid line in Figure 6). A mean value coordinate interpolation scheme (23) is chosen to produce a smooth deformation of the rectum mesh.

Deformation of the centre line

The material properties of soft tissues are complicated: stress/force may non-linearly depend on strain/displacement, changing rate and history of strain/displacement (24–26). Most material tests used animal tissues: Gregersen *et al*. (27) studied the material properties of guinea-pig small intestine; Watters *et al*. (28) tested the samples of rat colon; and Kawamura *et al*. (29) reported their tensile test of porcine large intestine. Rosen *et al*. (25) provided a complete analysis of constitutive relations of porcine abdominal organs, including liver, stomach, gallbladder, small intestine and large intestine. They proposed to use the EXP2 model

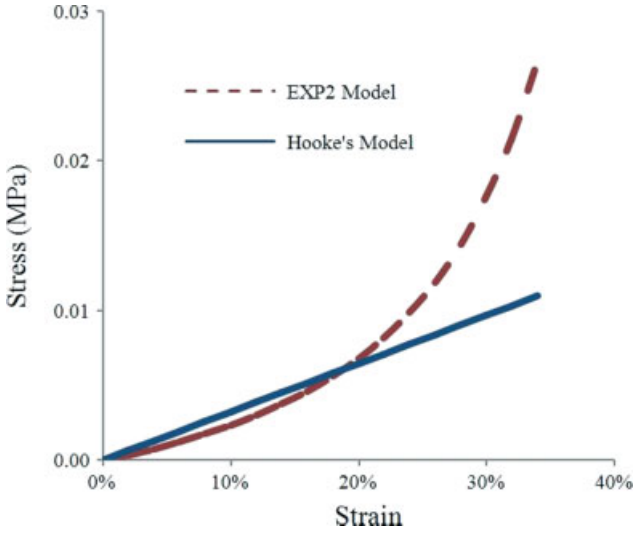

Figure 7. Linear and non-linear elastic tissue models

of hyperelasticity to describe the constitutive equations, where the stress is proportionally related to the exponent of strain square by fitting the experimental data. It is not practical to apply the EXP2 model to achieve real-time performance for our surgical simulation, simply because the computational burden is beyond the capacity of available computing resources. Instead, we chose to use the linear elastic Hooke's model with Young's modulus of 32.3 kPa and the Poisson ratio set to 0.35, which provides a good match to the non-linear model when the strain is small (<22%), as shown in Figure 7. Due to lack of access to the experimental data of human tissue, the material property we used was estimated by fitting the test results of porcine large intestine (25), where the strain value is in the range 0–0.20. The Young's modulus can increase dramatically with larger strain; e.g. Young's modulus of 270–510 kPa was observed in the breaking test (29). In our simulation, the extreme situation of breaking is not of concern, since only gentle forces are applied to the tissue during the surgery to avoid damage or bleeding. Watters *et al*. (28) reported the Young's modulus of rat colon for a lower strain range as 13.8–35.5 kPa, where they thought that the strain range was more in the physiological range than that in the breaking test. Our estimation converges well with the report of Watters *et al*. It was noticed that the material properties may vary individually, due to the age and other conditions. Observing real surgery practices from our surgeon colleagues confirms that most manipulations on the membranes and fat tissues can be satisfactorily modelled with this linear constitutive model.

As illustrated in Figure 6, we proposed to calculate the deformation of the centre line of the rectum, which was used to drive the shape changing of the whole structure via the cage layer. With the Cosserat rod model, an object is described by a flexible curve with a local coordinate frame attached to each point on the curve, where the rotation of the local frame stands for the rotation of the cross-section of the object at the location. A dual ($\mathbf{r}$, $< \mathbf{d} >$) describes the state of the rectum, where $\mathbf{r}$ is the global coordinate of

the material point and $<\mathbf{d}>$ denotes the three directors of the local coordinate frame. Taking the above notation, we are able to evaluate the shape change of the rod as its local flexures, the torsion around its tangent direction and stretch (30), change. It is feasible to treat the problem as a semi-static one by omitting the influence of the inertial force. The dual ($\mathbf{r}$, $<\mathbf{d}>$) which defines the shape of the rectum can be solved by minimizing the potential energy, with consideration of the available geometric and physical constraints applied. Theetten and Grisoni (31) provided a good summary of the Lagrangian multiplier method with constraints. The potential energy of the rod is written as follows:

$$\Pi = \frac{1}{2}\int [EI(\Delta\kappa_1{}^2 + \Delta\kappa_2{}^2) + GJ\Delta\tau^2 + EA\Delta\varepsilon^2]ds - \int \mathbf{f}\cdot\Delta\mathbf{r}ds \quad (5)$$

where $\frac{1}{2}\int EI(\Delta\kappa_1{}^2 + \Delta\kappa_2{}^2)ds$ is the elastic energy caused by bending, with $\Delta\kappa_1$ and $\Delta\kappa_2$ measuring the flexure changes in two orthogonal directions in the cross-section, E is the Young's modulus, I is the moment of inertia of the cross-section, $\frac{1}{2}\int GJ\Delta\tau^2 ds$ is the elastic energy related to torsion with $t\Delta\tau$ measuring the torsion of the given section, G is the shear modulus, J is the polar moment of inertia, $\frac{1}{2}\int EA\Delta\varepsilon^2 ds$ is the elastic energy related to the length change of the rectum, with $\Delta\varepsilon$ measuring the length change and A as the area of cross-section, $\int \mathbf{f}\cdot\Delta\mathbf{r}ds$ is the work done by the external force $\mathbf{f}$ and $\mathbf{r}$ is the location of material points on the curve. All the above integration is along the whole curve length.

When presenting the curve into n individual sections with $n+1$ nodes, the energy can be expressed by the summation of discretized node values. Minimization of the potential energy gives the solution of a rod in equilibrium by solving the linear equations with unknowns on the discretized nodes. Far more details about the discretization can be found in (32). In the next section, a method to map deformation of a single curve onto a mesh of the true shape of rectum is developed.

Cage construction and deformation

To preserve the volume during deformation, here we adopted a similar technique to the cage-based deformation from Ju *et al.* (32). We built up a cage at the binding pose where the whole intestine was fully extended. The deformation of the intestine followed two steps: first, when the cross-rod model deformed the centre line, each vertex of the cage was recomputed; second, the deformed cage drove the deformation of the surface mesh.

For the rectum model (Figure 8a), only two types of cross-section polygons (sphere template and middle template) were used for the cage. The sphere template polygon was placed at the centre of each sphere and a ring of vertices was distributed evenly on the sphere surface. The middle template polygon was placed on the centre line between two adjacent spheres; it held the same number of vertices as the adjacent sphere cross-sections. The cage was constructed at the rest pose where the whole intestine was fully extended. At each sphere centre, a cross-section template was located. At each middle point between two adjacent spheres, the middle template was located along the local frame of the centre line. Then each vertex had to be extended in the normal directions to be attached to the surface of the intestine model. As the difference between the local frames of adjacent template was not big, it was very easy to connect the corresponding vertices to form the embedding cage. To ensure proper cage deformation, the intestine mesh should be 'embedded' inside the cage. However, the current cage was still intersected with the mesh, as shown in Figure 8b. So, for all the vertices on the cross-section templates, we extended them along the local normal direction a small distance to make sure the cage loosely wrapped the surface of the intestine (Figure 8c).

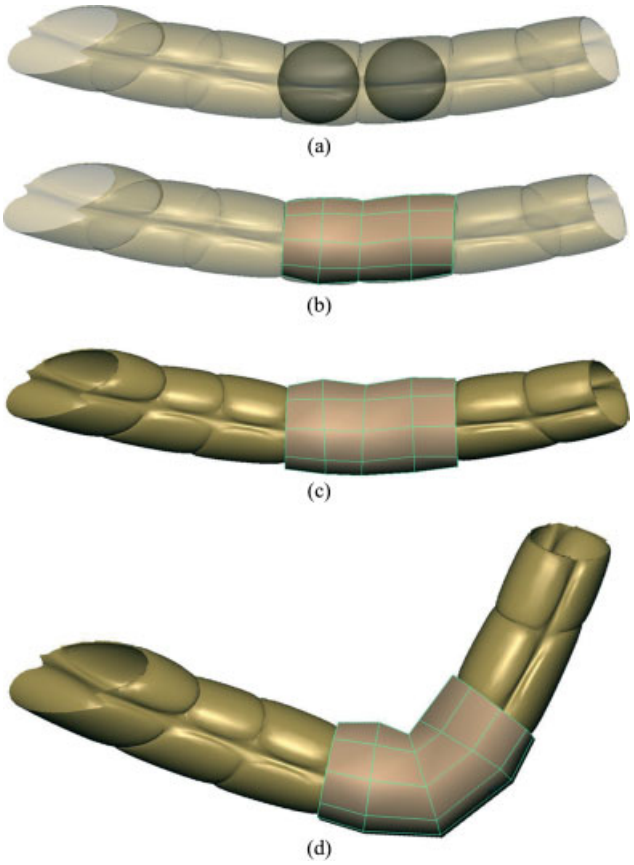

Figure 8. Cage construction and deformation: (a) locating cross-section templates; (b) initial tight cage; (c) final cage; (d) cage-based intestine deformation

After the cage was set up, we can use the cage-based deformation techniques to deform the intestine surface. Since the intestine was bound to the cage in the fully extended shape, the cage in the rest pose was roughly convex; and because the intestine was fully embedded inside the cage, in our implementation, to achieve the highest efficiency, we adopted mean value coordinates (23) to deform the intestine surface.

Considering the local effect of the cage on the intestine surface deformation, we only considered the vertices on the adjacent templates area for calculating the coordinates. This local optimization strategy reduces the computation complexity further in the cage deformation.

During deformation, each sphere was transformed and reorientated according to the centre line. The new shape of the cage could then be easily computed. Then the deformed intestine surface was determined. As cage deformation and cross-section deformation are very efficient, this skinning process could be performed in real time. Figure 8d gives the results of intestine model bending. Since only rotation operations are involved in the computation of template vertices, the volume of the intestine was largely preserved.

Collision detection

Collision detection can be easily handled with our hybrid deformation model. The spheres were used to detect the collision as bounding spheres. The use of bounding volume in collision detection is not new and some similar approaches were implemented (7,8). In (7), a penalty method was used. In our system, we used a geometric projection method to handle the collision, which directly corrected the positions of spheres after a contact was detected. In our method, there was no need to compute the penalty forces and hence the solving process was speeded up. In the projection method, simply when intersection of the bounding volume happens, a correction was directly applied to move the object (bounding volume) to clear the occlusion. The direction of the movement was decided as the normal of the intersection plane. A few iterations of the correction were performed to minimize the occurrence of intersections, as the previous correction may introduce new intersections. Occasionally we might experience local inconsistency, as the intersection could not be corrected, but in most cases it was resolved in the next few frames in the simulation. This only caused a negligible loss in image quality. A simple diagram is given in Figure 9.

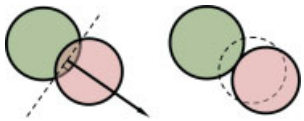

Figure 9. Illustration of collision handling

Simulation of real-time cutting

Cutting is an essential procedure in laparoscopic colorectal surgery. Since cutting requires real-time remeshing of the model, which can increase the computation complexity significantly, interactive realistic cutting simulation is always a challenging topic in virtual reality-based medical simulation and has attracted a great deal of research effort. Moreover, for haptic rendering, simulation of the physical cutting process is also a complex research topic and system stability is important. Sela *et al*. (33) developed an FEM-based incision algorithm using the discontinuous free-form deformation method. They modelled the soft tissue and split the model surface by changing the topology of the geometry. Bielser *et al*. (34) used a look-up table to reduce the computation cost and new polygons were created for the cutting area. Choi *et al*. (5) presented a real-time cutting algorithm based on the hierarchical approach for the mixed model (BEM + surface mesh) in the laparoscopic oesophagus surgery simulator.

Most cutting algorithms (35–37) need to change the model topology. Modification of topology is usually a very time-consuming computation step. In this paper, to ensure real-time performance, we present a surface mesh-based cutting algorithm with little topology modification. Inspired by the hierarchical strategy (5), we used a hierarchical database to deal with the mesh subdivision in order to improve the computation efficiency.

Cutting procedure

Once the contact between the cutting instrument and the initial intersecting triangle of the intestine surface mesh is detected, the position (3D coordinates) of the contact point will be recorded when the penetration occurs. The system then determines whether the cutting instrument moves across any edge of this initial intersecting triangle. If the answer is 'yes', the cutting algorithm divides this triangle into several sub-triangles. The neighbour triangle that shares the edge with the initial triangle is added to the cutting list for the next triangle to be processed. During triangle subdivision, a hierarchical database (5) is constructed to record the relationship between each original triangle and its subdivided triangles. Finally, when the simulator detects the cutting instrument untouched with the intestine model surface, the position of this point is recorded. The triangle with this point is added to the cutting list as the last triangle for subdivision. To preserve the edge information of the original mesh, the edge information and mass-spring model of the mesh is updated every time when a cutting operation is complete. Figure 10 shows the flowchart of this procedure.

Cutting modelling

Technically, there are two stages of the interaction between the surgery cutting instrument and the object surface when cutting a piece of tissue. First of all, the instrument penetrates into the tissue and the tissue will be opened. Then, the instrument will be moved when its tangential force exceeds the static cut friction. Here, we use the following force model to describe the haptic behaviour of cutting (Figure 11):

$$\vec{F} = \vec{F}_t + \vec{F}_n \tag{6}$$

DOI: 10.1002/rcs

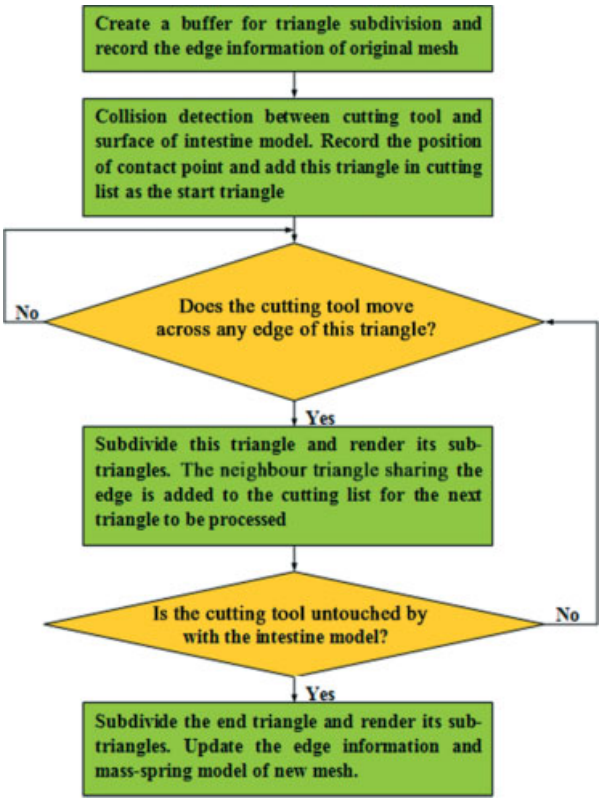

Figure 10. Flowchart of the cutting algorithm

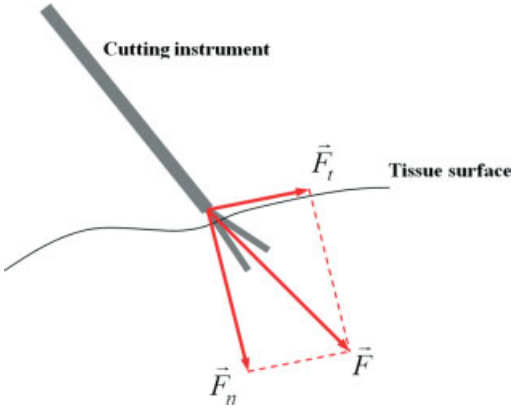

Figure 11. Decomposition of force in cutting

where $\vec{F}$ is the external force applied by the user to the surface of the tissue concerned. $\vec{F}$ can be decomposed into a tangential force, $\vec{F}_t$, on the surface and a normal force, $\vec{F}_n$, perpendicular to the surface. $\vec{F}_t$ is responsible for the incision movement of the instrument on the surface; $\vec{F}_n$ controls the pressing force of cutting instrument on the tissue surface. In our system, when the cutting mode is selected by the user, the following criterion is used to determine whether or not the cutting starts:

$$\left|\vec{F}_n\right| > F_{penerate}, \quad \left|\vec{F}_t\right| > F_{static-friction} \tag{7}$$

In (7) the instrument will open the tissue only if the magnitude of $\vec{F}_n$ is larger than a given tissue-dependent threshold, $F_{penerate}$. Then, if the magnitude of $\vec{F}_t$ exceeds the value of static friction of tissue, $F_{static-friction}$, the instrument will start cutting.

During cutting, the system will monitor the value of $\vec{F}_t$ in each haptic frame. If $\left|\vec{F}_t\right|$ is larger than the dynamic friction $F_{dynamic-friction}$, the cutting instrument moves. When the instrument is untouched by the tissue surface, the cutting ends. For this process, all the parameters: $F_{penerate}$, $F_{static-friction}$ and $F_{dynamic-friction}$ can be set by the surgeon.

Stability analysis

In 3D interaction, stability analysis of virtual environments is an open problem. Since not all hardware parameters are the same and are known to the developers, it is difficult to establish a general stability criterion for a phantom device-based system. Moreover, with the deformation of soft tissues and the updating of 3D motion information of the virtual surgery instruments in each haptic frame, the virtual force mapping is usually a non-linear problem (38). Based on the virtual wall model and passive characteristics of proxy in contact, energy accumulation of motor output and violation of passive dynamic criteria are considered to be the factors that affect system stability (39). When the passive dynamics criteria are violated, unstable interaction will happen. Then force continuity will be broken, leading to vibration.

According to the control theory, a non-linear system can be transformed into a linear system at a local working point. Similarly, the cutting process can be described as a series of several contact states. Based on the interaction state transition model, the stability of the cutting process can be divided into two stages. The first is the stability in each contacting phase; the second is the stability at the transition time between two contacting states. Colgate *et al*. (38) presented a Z-width criterion, which selects the impedance of the virtual environment as the criterion for the system's stability. In our haptics-based simulation system, the Z-width criterion is adopted as the condition to maintain system stability. For the first stage of stability, the following criterion should be satisfied:

$$K < \frac{2(b-B)}{T} \tag{8}$$

where b is the inherent damping of the haptic device, K, B are the stiffness and damping of the virtual tissue, T is the time interval between adjacent haptic frames (about 1 ms) and $\frac{2(b-B)}{T}$ is the upper limit of virtual stiffness, which can be measured by experiments. Moreover, for the second stage of stability, the following criterion (40) should be satisfied:

$$K_m > -\frac{KF}{\delta} \tag{9}$$

where K_m is the coefficient of removing material elements from the tissue and δ is a finite small value defined by the developer. When both equations (8) and (9) are satisfied, the haptic system is stable during simulation.

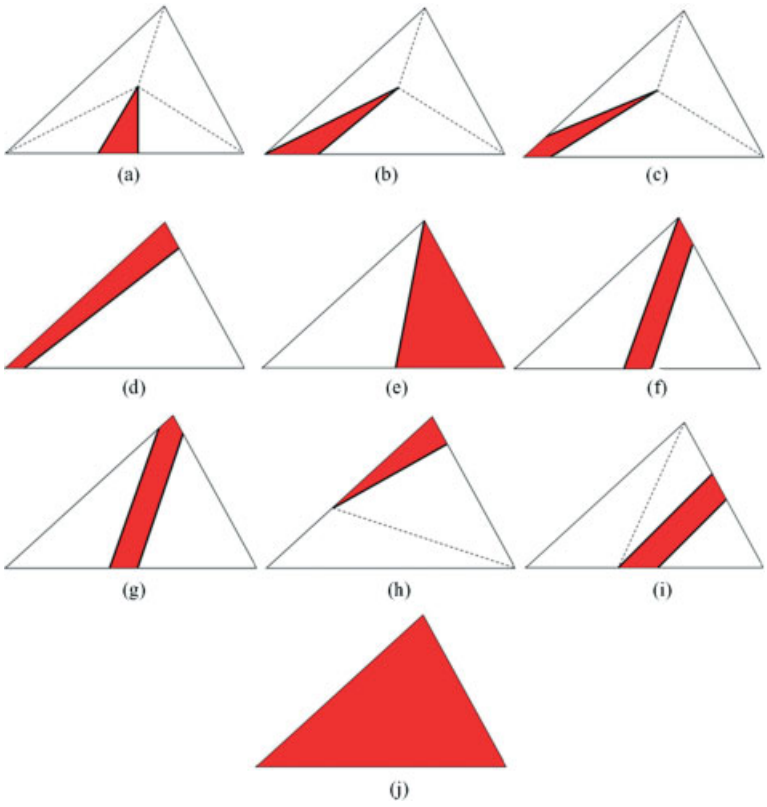

Figure 12. Five cases for triangle subdivision

Triangle subdivision

Mesh subdivision is an important research topic in computer graphics. It could be computationally very expensive, becoming a bottleneck for achieving real-time performance. In this paper, we present a simple but very efficient subdivision strategy by considering the possible triangle split patterns. Categorizing the possible patterns of triangle subdivision is crucial for creating a fast subdivision algorithm.

Triangle split is enumerated into 10 subdivision cases, considering both symmetry and rotation transformation (Figure 12). For the start and end triangles (the initial and the last triangles on the cutting list), there are three cases (Figure 12a–c). Figure 12a illustrates the case that none of the three vertices in a triangle is in the cutting region; Figure 12b illustrates the case where one of the three vertices is on the edge of the cutting region; Figure 12c illustrates the cases where one of the three vertices is in the cutting region.

For the connecting triangles (the triangles between the start and end triangles on the cutting list), there are seven cases (Figure 12d–j). Figure 12d, e illustrates the case where two of the three vertices are in the cutting region; Figure 12f–h illustrates the case where one of the three vertices is in the cutting region; Figure 12i shows none of the three vertices is in the cutting region; and Figure 12j illustrates the case where all the vertices are in the cutting region.

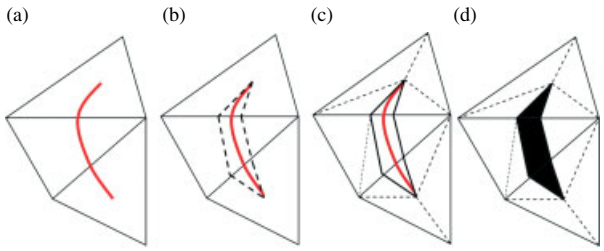

Figure 13. Triangle subdivision example

During subdivision, when a triangle is split, the triangle itself is not displayed. Instead, the subdivided sub-triangles are rendered and saved in a hierarchical database. Figure 13 gives a simple example of triangles subdivison; the red curve is the route of a surgical instrument. Figure 13d illustrates the final result of the triangles subdivision.

Element removal and mesh simplification

During cutting simulation, isolated triangles may be generated when the cutting route intersects. Due to gravity, these isolated triangles will drop and be removed automatically by the system, as they are not connected with the fixed nodes (vertices) in the mass-spring mode. In addition, after several cutting manipulations, the surface mesh model may contain many small obtuse triangles. To improve mesh quality and computation efficiency for later

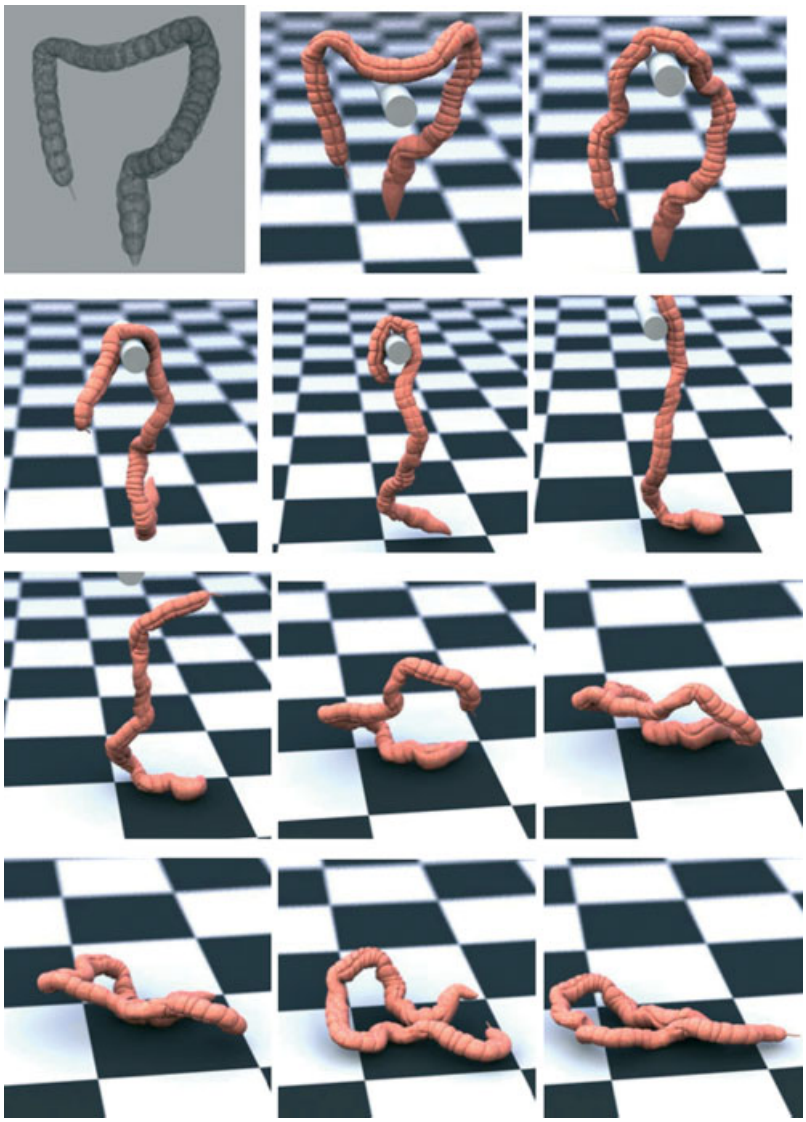

Figure 14. Deformation and collision detection for an intestine model falling to the ground

processing, a mesh simplification method (35) is used in this simulator. We adopt the edge-collapse algorithm to re-mesh the part of the soft tissue surface with poorly shaped triangles. When these small obtuse triangles are found, the shortest edge will be selected and collapse to remove these triangles. Currently, the criterion for mesh simplification simply checks whether the average size of the sub-triangles is less than one-eighth of its original size. As mesh simplification only focuses on the sub-triangles, not the whole mesh, it only considers a small number of triangles around the cutting region. Most triangles that are far away from the cutting region do not need to be considered during the simplification. Therefore, it does not really increase the computation cost.

Results

Implementing the above techniques, we have developed a prototype VR-based simulation system for laparoscopic rectum surgery. Once the simulator starts, the system generates a continuous force-feedback loop. The haptic device sends the orientation and position parameters to the computer. Collisions between surgical instruments and the intestine surface are detected according to these data. The deformation of soft tissue and force is computed by the hybrid mechanical model. Finally, the feedback force signal is sent to the haptic device for haptic rendering. Our system runs on a Workstation with Intel CoreQuad 2.83 GHz, 3 GB memory and equipped with an nVidia Quadro FX 3700 graphics board. The computer handles all computations, including deformation, collision detection, cutting and rendering. The force-refreshing frequency is 1200 Hz and the graphic refreshing frequency is 33 Hz.

To evaluate the effectiveness of the techniques in this simulator, we have also designed two experiments. The first tests the visual performance of the deformation and collision detection algorithm. To assess this process more directly, we have implemented the algorithm with the animation software Maya and use an animation video to illustrate its performance. Here, a hung intestine model

DOI: 10.1002/rcs

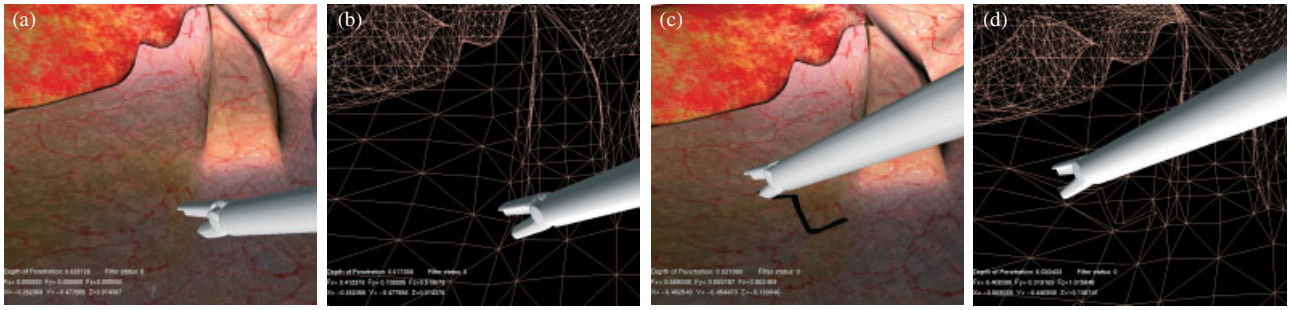

Figure 15. Results of real-time cutting simulation: (a) texture of the intestine model before cutting; (b) mesh of the intestine model before cutting; (c) texture of the intestine model after cutting; (d) mesh of the intestine model after cutting

falls down to the ground. Figure 14 gives some screen shots: the first figure outlines different layers of the hybrid model; the following 11 figures are from frame 1 to frame 44 with intervals of three frames.

From the experimental results shown in Figure 14, we found the deformation performance to be plausible. The collision detection between the intestine and the ground and the self-collision of the intestine are both effectively solved. Our second experiment was the real-time cutting algorithm. Figure 15 gives the results. From Figure 15d, we could see that the mesh was correctly subdivided.

Discussion

Throughout the whole system developmental process, three consultant surgeons from the Bournemouth and Poole Hospitals (NHS, UK) have been closely involved. They both advised us about the medical content and helped to evaluate the results. A satisfactory tactile feedback was achieved, according to their experience. With haptic rendering, trainees can inspect the internal operation environment with realistic tactile feeling and real-time visual outputs.

Conclusion and Future Work

We have developed a prototype virtual reality simulator for laparoscopic rectum surgery. A number of technical innovations have been presented in this paper, including a haptic force filter, soft tissue deformation computation, collision detection and real-time cutting. Realistic haptic rendering was performed and real-time performance was achieved. Our surgeon collaborators were satisfied with the tactile feedback and visual quality of our prototype system.

Despite successful implementation of the prototype, our system also had a number of limitations. To simplify the computation, we used surface mesh to model the intestine with one layer. In fact, intestinal tissues consist of a number of different layers. To simulate the mechanical behaviour of a multi-layered structure, a true multi-layered intestine model with different material properties would represent the behaviour more accurately. Currently, our haptic rendering for the cutting operation is relatively simple. As Phantom Omni gives the user only a three-DOF force feedback, the cutting force feedback is approximated with a force vector and the torque is not considered during the virtual operation training process. A button on the haptic device is used to start the cutting mode and the cut surface is generated by mesh subdivision. In real surgery training, proper cutting torque is required. In future, we plan to use a more complex and expensive haptic device with not only force but also torque feedbacks to increase the tactile realism for cutting simulation. Finally, some auxiliary functions, such as the visual effect of bleeding, will be added. An operation guidance strategy that can evaluate the level of competence of the trainee will also be also incorporated.

Acknowledgements

The authors would like to thank Wenxi Li for his animation video in this project. The research in this paper was supported by a grant from the Royal Bournemouth and Christchurch Hospitals NHS Trust and The Higher Education Innovation Fund (HEIF) grant from Bournemouth University.

References

1. Francone T, Weiser MR. Laparoscopic rectal resection for cancer. *Semin Colon Rect Surg* 2005; **16**(3): 147–154.
2. http://www.cae.com/en/healthcare/laparoscopy.asp
3. http://www.mentice.com/
4. Heng PA, Cheng CY, Wong TT, *et al*. A virtual reality training system for knee arthroscopic surgery. *IEEE Trans Informat Technol Biomed* 2004; **8**(2): 217–227.
5. Choi C, Kim J, Han H, *et al*. Graphic and haptic modeling of the oesophagus for VR-based medical simulation. *Int J Med Robotics Comput Assist Surg* 2009; **5**: 257–266.
6. Li H, Leow WK, Chiu IS. Elastic tubes: modeling elastic deformation of hollow tubes. *Comput Graphics Forum* 2010; **5**: 227–236.
7. France L, Lenoir J, Angelidis A, *et al*. A layered model of a virtual human intestine for surgery simulation. *Med Image Anal* 2005; **9**(2): 123–132.
8. France L, Angelidis A, Meseure P, Cani MP, Lenoir J, Faure F, Chaillou C. Implicit Representations of the Human Intestines for Surgery Simulation. The Proceeding of *Modelling and Simulation for Computer-aided Medicine and Surgery (MS4CMS)*, November 2002; **12**: 42–47.
9. Raghupathi L, Grisoni L, Faure F, *et al*. An intestinal surgery simulator: real-time collision processing and visualization. *IEEE Trans Visualiz Comput Graphics* 2004; **10**(6): 708–718.

10. Chang J, Yang X, Zhang JJ. Continuous skeleton-driven skinning – a general approach for modelling skin deformation. *Int J Image Graphics* 2009; **9**(4): 591–608.
11. Lin MC, Otaduy M. *Haptic Rendering: Foundations, Algorithms and Applications.* A. K. Peters: Natick, 2008.
12. Otaduy MA, Lin MC. Sensation preserving simplification for haptic rendering. *ACM Trans Graphics* 2003; **23**(3): 543–553.
13. Galoppo N, Tekin S, Otaduy MA, *et al*. Interactive haptic rendering of high-resolution deformable objects. *Virtual Reality (LNCS)* 2007; **4563**: 215–223.
14. Basdogan C, De S, Kim J. Haptics in minimally invasive surgical simulation and training. *IEEE Comput Graphics* 2004; **24**(2): 56–64.
15. Wu J, Leung YS, Wang C, *et al*. Smooth force rendering on coarse polygonal meshes. *Comput Anim Virtual Worlds* 2010; **21**(3–4): 235–244.
16. Maciel A, De S. An efficient dynamic point algorithm for line-based collision detection in real time virtual environments involving haptics. *Comput Anim Virtual Worlds* 2008; **19**(2): 151–163.
17. http://www.mitk.net/
18. Mollemans W, Schutyser F, Cleynenbreugel J, *et al*. Fast soft tissue deformation with tetrahedral mass spring model for maxillofacial surgery planning systems. In Medical Image computing and Computer Assisted Intervention (MICCAI), 2004; Springer-Verlag, Berlin, Heidelberg; 3217: 371–379.
19. Hong M, Jung S, Choi M, *et al*. Fast volume preservation for a mass-spring system. *IEEE Comput Graph Appl* 2009; **26**(5): 83–91.
20. Bathe KJ. *Finite Element Procedures*, 2nd edn. Prentice-Hall: London, 1996.
21. Wu W, Heng PA. A hybrid condensed finite element model with GPU acceleration for interactive 3D soft tissue cutting. *Comput Anim Virtual Worlds* 2004; **15**(3–4): 219–227.
22. Antman S. *Nonlinear Problems of Elasticity*. Springer-Verlag: New York, 1995.
23. Ju T, Schaefer S, Warren J. Mean value coordinates for closed triangular meshes. *ACM Trans Graph* 2005; **24**(3): 561–566.
24. Hoeg HD, Slatkin AB, Burdick JW, *et al*. Biomechanical modeling of the small intestine as required for the design and operation of a robotic endoscope. The Proceeding of *2000 IEEE International Conference on Robotics and Automation (ICRA)* 2000; 1599–1606.
25. Rosen J, Brown JD, De S, *et al*. Biomechanical properties of abdominal organs *in vivo* and postmortem under compression loads. *J Biomech Eng* 2008; **130**(2): 21–29.
26. Basdogan C, Sedef M, Harders M, *et al*. VR-based simulators for training in minimally invasive surgery. *IEEE Comput Graphics* 2007; **27**(2): 54–66.
27. Gregersen H, Emery JL, McCulloch AD. History-dependent mechanical behaviour of guinea-pig small intestine. *Ann Biomed Eng* 1998; **26**(5): 850–858.
28. Watters DA, Smith AN, Eastwood MA, *et al*. Mechanical properties of the rat colon: the effect of age, sex and different conditions of storage. *J Exp Physiol* 1985; **70**(1): 151–162.
29. Kawamura Y., Naemura K. Breaking strength of porcine large intestines. *Trans Jpn Soc Mech Eng A* [in Japanese] 2009; **75**(756): 1124–1126.
30. Chang J, Pan J, Zhang JJ. Modelling rod-like flexible biological tissues for medical training. Workshop on 3D Physiological Human, 29 November–2 December 2009, Zermatt, Switzerland; 51–61.
31. Theetten A, Grisoni L. A robust and efficient Lagrangian constraint instrument kit for the simulation of 1D structure. *Comput Aided Design* 2009; **41**(12): 990–998.
32. Ju T, Zhou QY, Panne M, *et al*. Reusable skinning templates using cage-based deformations. Proceedings of Siggraph Asia 2008. *ACM Trans Graphics* **27**(5): 1–10.
33. Sela G, Subag J, Lindblad A. Real-time haptic incision simulation using FEM-based discontinuous free-form deformation. *Comput Aided Design* 2007; **39**(8): 685–693.
34. Bielser D, Gross MH. Interactive simulation of surgical cuts. In The Eighth Pacific Conference on Computer Graphics and Applications, 2000; 116–125.
35. Ganovelli F, O'Sullivan C. Animating cuts with on-the-fly re-meshing. Eurographics, Manchester, UK, 2001; 243–247.
36. Picinbono G, Lombardo JC, Delingette H, *et al*. Improving realism of a surgery simulator: linear anisotropic elasticity, complex interactions and force extrapolation. *J Vis Comput Animat* 2002; **13**: 147–167.
37. Cotin S, Delingette H, Ayache N. A hybrid elastic model for real-time cutting, deformations, and force feedback for surgery training and simulation. *Visual Comput* 2000; **16**(8): 437–452.
38. Colgate J, Brown J. Factors affecting the Z-width of a haptic display. In Proceedings of the IEEE International Conference on Robotics and Automation, 1994; 3205–3210.
39. Wang D, Zhang Y. Effect of haptic device's position resolution on stability. In Proceedings of EuroHaptics 2004; 377–380.
40. Wang D, Zhang Y, Wang Y, *et al*. Cutting on triangle mesh: local model-based haptic display for dental preparation surgery simulation. *IEEE Trans Vis Comput Graph* 2005; **11**(6): 671–683.